Article

Micropositioning and Fast Transport Using a Contactless Micro-Conveyor

Guillaume J. Laurent *, Anne Delettre, Rabah Zeggari, Reda Yahiaoui, Jean-François Manceau and Nadine Le Fort-Piat

FEMTO-ST Institute, UFC-ENSMM-UTBM-CNRS, Université de Franche-Comté, Besançon 25000, France; E-Mails: anne.delettre@femto-st.fr (A.D.); rabah.zeggari@femto-st.fr (R.Z.); reda.yahiaoui@femto-st.fr (R.Y.); jfmanceau@femto-st.fr (J.-F.M.); nadine.piat@ens2m.fr (N.L.F.-P.)

* Author to whom correspondence should be addressed; E-Mail: guillaume.laurent@ens2m.fr; Tel.: +33-3-8140-2808; Fax: +33-3-8140-2809.

Abstract: The micro-conveyor is a 9×9 mm^2 manipulation surface able to move millimeter-sized planar objects in the four cardinal directions using air flows. Thanks to a specific design, the air flow comes through a network of micro-channels connected to an array of micro-nozzles. Thus, the micro-conveyor generates an array of tilted air jets that lifts and moves the object in the required direction. In this paper, we characterize the device for transport and positioning tasks and evaluate its performances in terms of speed, resolution and repeatability. We show that the micro-conveyor is able to move the object with a speed up to 137 mm$\cdot$s^{-1} in less than 100 ms whereas the positioning repeatability is around 17.7 μm with feedback control. The smallest step the object can do is 0.3 μm (positioning resolution). Moreover, we estimated thanks to a dynamic model that the speed could reach 456 mm$\cdot$s^{-1} if several micro-conveyors were used to form a conveying line.

1. Introduction

Transporting and positioning are very common task in manufacturing. As the objects being manipulated become smaller and smaller when speed increases, standard devices as conveyor belts show

some limitations, and it also becomes difficult to pick and place objects at the right position. To get around the difficulty, other methods such as distributed manipulation have been introduced. Distributed manipulation systems induce motions on objects through the application of many external forces by pushing, sliding or blowing [1]. Researchers designed and built actuators arrays that can be used for positioning, conveying, feeding and sorting planar objects. Arrayed systems can be divided into two categories: contact systems and contactless systems.

Contactless systems mainly use air-flow levitation. They have several advantages including high velocities and removal of friction problems. The Xerox PARK paper handling system [2,3] uses 1152 tilted air-jets in a 12 in × 12 in array to levitate paper sheets. The levitation-transport system uses two arrays of 578 valves arranged in opposition to one another across a small gap in which the paper is located. The system has demonstrated closed-loop positioning accuracy of 0.05 mm and trajectory tracking with typical speed of 30 mm·s^{-1}. Kim and Shin [4] also used an array of tilted air jets to move wafers in their clean-tube system. The device was developed as a means of transferring and positioning wafers inside a closed tube filled with super clean air. Speed and positioning repeatability are not precisely investigated but the orders of magnitude are respectively 50 mm·s^{-1} and 0.1 mm. At a smaller scale, some active surfaces have been developed using MEMS actuator arrays [5–7]. The Fukuta's device is able to produce tilted air-jets thanks to integrated electrostatic valves. In their experiments a flat plastic object was successfully moved with a speed of 4.5 mm·s^{-1}. Luntz and Moon [8,9] introduced another principle based on potential air flow to move an object on an air-hockey table. They proposed a manipulation methodology that allows to move an object to a unique final pose using airflow fields without sensors. Laurent *et al*. [10,11] used the proposed traction principle to move a product thanks to an array of vertical air jets which induce desired potential air flow over the surface. This device is able to move centimeter-sized objects up to 200 mm·s^{-1} with millimetric closed-loop positioning accuracy.

Most of these arrayed systems use individually controllable actuator arrays. The movement of each individual actuator is controlled to get continuous motion of a single object or several objects. They integrate a large number of actuators in one device that increases the risk of failures and reduces the maintainability in a industrial context.

In a previous paper, Yahiaoui *et al*. proposed a micro-conveyor concept and its implementation which may be useful for the manipulation of small planar objects [12]. The micro-conveyor consists of a stack of three layers, two silicon wafers and a lower Pyrex glass wafer. The top side of the upper silicon wafer represents the manipulation surface and includes an array of 8 × 8 square holes with four nozzles each (cf. Figure 1). Its bottom side includes 16 micro-channels which supply the south and north nozzles. 16 other micro-channels which supply the east and west nozzles are etched in the bottom side of the middle wafer. The Pyrex wafer is used to seal hermetically the micro-channels of the middle wafer. Four holes machined in the Pyrex allows for connecting the channels to the air source by means of glued industrial connector. The micro-conveyor has been designed to generate an air jet with an angle of 45° from the vertical [13,14]. The orientation of the air jets is due to the shift of the holes in the upper wafer. As a result when supplied in one of the four inlets, the micro-conveyor produces an array of 64 tilted air jets that lifts and moves an object in the according direction (cf. Figure 2) at the same time.
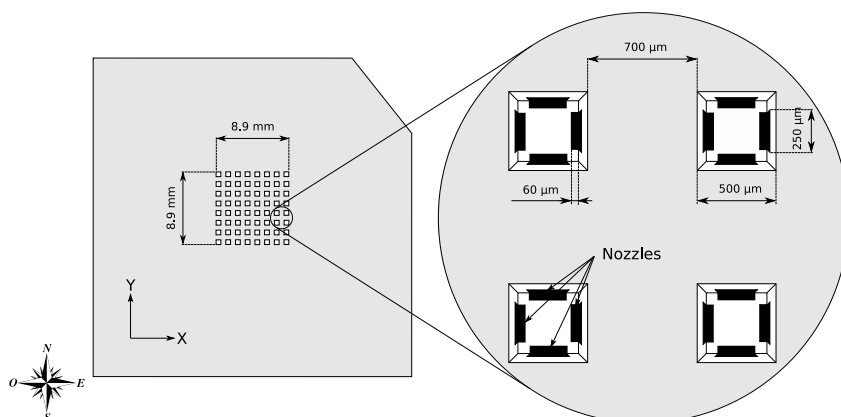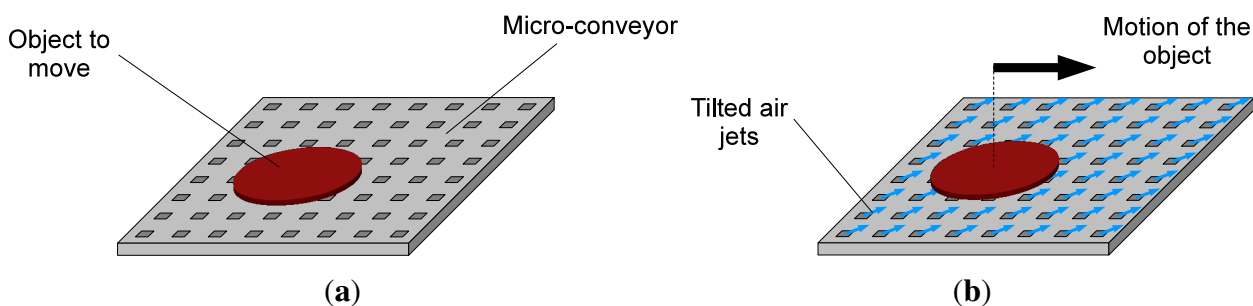
Figure 1. Top side of the micro-conveyor.

Figure 2. Working principle of the micro-conveyor. (**a**) Neutral position (non-blowing); (**b**) Blowing to the east direction.

(**a**)   (**b**)

This micro-conveyor is expected to have several advantages over conventional methods. Using an array of air jets to handle small objects has the advantage of not requiring precision gripping nor a particular contact configuration which may be difficult to obtain for small objects. During the motion, no friction force occurs thanks to the aerodynamic levitation of the object. This may be useful for very fast manipulation.

In this paper, we test the manipulation device and evaluate its performances thanks to the modeling of the dynamics of an object. The next section describes the characterization of the flow. The third part explores the transporting capabilities of the device. The last section presents the experimental determinations of the positioning resolution in open loop and the positioning repeatability in closed loop.

2. Characterization of Flow

Before characterizing the motion of an object over the micro-conveyor, we measured the volumetric flow to determine the head losses in the device and the velocity of the outgoing air.

As the used pressures are only several kilopascals near atmosphere, we can consider that the fluid is incompressible. The momentum equation reduces to Bernoulli's equation. Neglecting the gravity, we have:

$$\frac{U^2}{2} + \frac{P}{\rho} = \text{constant} \quad \text{(along a stream line)} \tag{1}$$

where U and P are respectively the speed and the pressure at a given point on a streamline, ρ is the density of the fluid at all points in the fluid.

Considering that the internal fluid is motionless ($U_i = 0$) and the relative external pressure is zero ($P_e = 0$), this equation gives the exit speed U_e knowing the internal pressure P_i before the output nozzle:

$$\frac{U_e^2}{2} = \frac{P_i}{\rho} \tag{2}$$

Due to head losses, P_i is far below the supply pressure P_0. Head loss is divided into two main categories: "major losses" associated with energy loss per length of pipe, and "minor losses" associated with bends, fittings, valves, *etc*.

The most common equation used to calculate major head losses is the Darcy-Weisbach equation:

$$\Delta_{major} = \frac{1}{2}\rho\frac{L}{D_h}\Lambda U_p^2 \tag{3}$$

where Δ_{major} is the pressure loss due to friction (in Pa), L is the length of the pipe (in m), D_h is the hydraulic diameter of the pipe (in m) defined by $D_h = \frac{4s}{p}$ with s the section of the pipe and p the perimeter of the pipe, U_p is the average speed of the fluid flow (in $\text{m} \cdot \text{s}^{-1}$) and Λ is a dimensionless coefficient called the Darcy friction factor.

For laminar (slow) flows, it is a consequence of Poiseuille's law that $\Lambda = 64/Re$, where Re is the Reynolds number. So, for laminar flows, the major losses are simply defined by:

$$\Delta_{major} = 32\frac{\mu L}{D_h^2}U_p \tag{4}$$

where μ is the dynamic viscosity of the fluid (in $\text{Pa} \cdot \text{s}$).

Minor losses are commonly calculated by the following equation:

$$\Delta_{minor} = \frac{1}{2}\rho K U_p^2 \tag{5}$$

where K is a dimensionless coefficient called the head loss coefficient.

To calculate the exit flow according to the supply pressure P_0, we need to write the pressure balance between P_i and P_0:

$$P_i = P_0 - \Delta_{major} - \Delta_{minor} \tag{6}$$

Using Equations (2), (4) and (5), we get:

$$\frac{\rho U_e^2}{2} = P_0 - 32\frac{\mu L}{D_h^2}U_p - \frac{1}{2}\rho K U_p^2 \tag{7}$$

The speed U_p of the fluid flow is equal to the volumetric flow rate Q per unit cross-sectional area S_p of the pipe:

$$U_p = \frac{Q}{S_p} \tag{8}$$

In the same way, we have $U_e = \frac{Q}{S_e}$ where S_e is the sum of the section areas of nozzles.

Finally, the volumetric flow rate Q is the solution of the equation:

$$\frac{1}{2}\rho\left(\frac{1}{S_e^2} + \frac{K}{S_p^2}\right)Q^2 + 32\frac{\mu L}{D_h^2 S_p}Q - P_0 = 0 \tag{9}$$

Given this equation and the flow measurements, we can determine the head losses in the micro-conveyor. For 10 values of supply pressure from 1 kPa to 10 kPa, we measured the volumetric flow thanks to a digital flowmeter. Then we calculated the values of losses that minimize the least squares error (LSE) between measurements and theory. The obtained curves and values are presented in Figure 3. It is noteworthy that if we consider only major losses or minor losses by setting one of the coefficient to zero, the shapes of the curves do not match. If we assume both major and minor losses the theory perfectly matches the measurements. The values of losses are similar in opposite directions. The value of losses are greater for the north-south directions due to the smaller size of channels inside the second layer [14].

Figure 3. Least squares fittings for each direction. (**a**) Flow *vs*. pressure; (**b**) Values of minor and major losses.
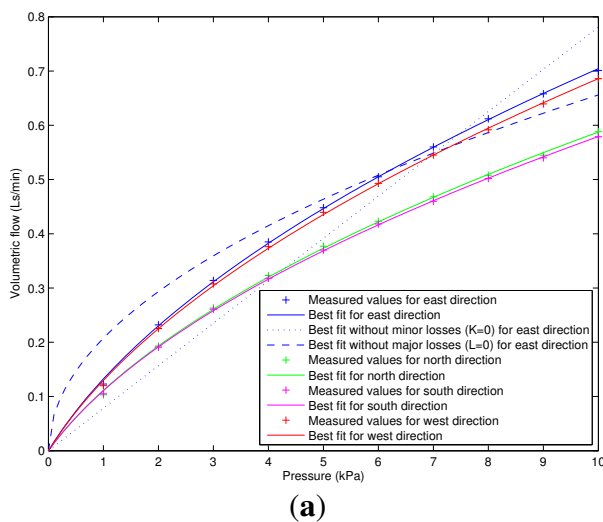
Direction	$\frac{K}{S^2}$	$\frac{L}{D_h^2 S}$	LSE
East	6.89×10^{13}	6.14×10^{11}	3.38×10^{-14}
East	0	1.30×10^{12}	8.94×10^{-12}
East	1.38×10^{14}	0	5.04×10^{-12}
North	1.00×10^{14}	7.24×10^{11}	3.44×10^{-14}
South	1.04×10^{14}	7.24×10^{11}	1.47×10^{-14}
West	7.33×10^{13}	6.24×10^{11}	4.13×10^{-14}

(**a**)   (**b**)

3. Transport Task

In this section, we evaluate the performances of the device for a conveyance task. The aim is to measure the trajectory and the speed of the object towards a direction.

3.1. Experimental Setup

The experimental setup consists of a pressurized air supply, pressure regulators, four on-off solenoid valves, an air tank, a firewire camera and a computer. Figure 4 shows the complete hardware configuration.

The micro-conveyor is put on a mechanical platform to adjust its position to the horizontal. The air-flow source is provided by compressed air via a digital proportional pressure control system. Each solenoid valve is independently actuated by an electric signal. Control signals are sent by computer via

a multi-channel digital output board and a 5 V/24 V amplifier circuit. An air tank is connected between the pressure regulator and the valves to damp the peaks of air consumption. The operating pressure is noted P_0.

**Figure 4.** Overview of the experimental setup.
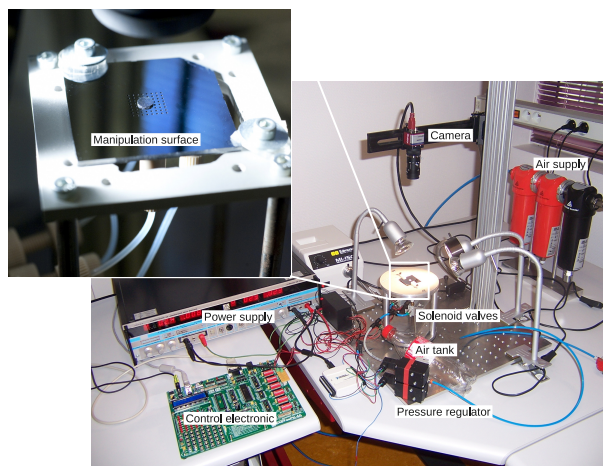
OpenCV library is used to measure the position of the object with the camera. OpenCV (Open Source Computer Vision Library) is a library of programming functions mainly aimed at real-time computer vision [15]. The position of the object is measured by the computation of the centroid of its pixels in order to get a subpixel resolution. The reference position $(0, 0)$ is defined as the center of the surface. The image processing is done at a rate of 60 frames per second.

The experiments has been done with a white-painted silicon cylinder of 5 mm in diameter and 0.4 mm in thickness. The mass m of the object is 19.43 mg.

3.2. Trajectory

The first experiments aim at the measurement of the motion of the object when a valve is open for a long time (step response). Before the experiment, the object is placed at the center of the surface. Then one of the valves is opened at time zero and we record the trajectory of the object thanks to the image processing described before. The object is lifted and accelerated, then leaves the active surface in about 100 ms. Figure 5 shows an image sequence of the experiment extracted from the video clip accompanying the paper.

Figure 5. Snapshots of the surface when the east valve is open at time 0. The operating pressure is $P_0 = 50$ kPa.

$t = 0$ ms　　　　　　　　　$t = 67$ ms　　　　　　　　　$t = 100$ ms
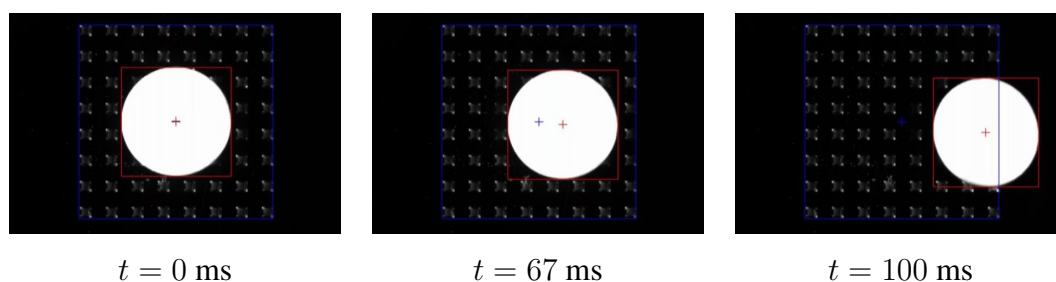
The first observation is that the path is not straight. To understand why, we carried out 20 trials in each direction (cf. Figure 6). An obvious cause of deviations could be the roll and pitch angles of the surface. However, in this case, the deviations should always be in the same direction and this is not the case. Actually, the reason of deviations is linked to the direction of the air jets themselves. As we wrote in the introduction, the design was determined to produce tilted air jets with an angle of 45° from the vertical. The validation of the design was conducted on a single nozzle in [13]. However, in this paper, one channel supplies a line of eight nozzles as shown in Figure 7. Fluid is transported through the channel with the axial velocity U_i. The volume flow balance gives:

$$Q_0 = U_0 S_p = U_1 S_p + U_{e,1} s_e = U_2 S_p + U_{e,1} s_e + U_{e,2} s_e = \cdots = \sum_{i=1}^{8} U_{e,i} s_e \qquad (10)$$

where S_p is the section area of the channel, s_e the section area of a nozzle and $U_{e,i}$ the exit speed of the flow through the nozzle i. So, the fluid decelerates in the downstream direction, *i.e.*,

$$U_0 > U_1 > \cdots > U_8 = 0 \qquad (11)$$

Figure 6. Trajectories of the object in the four directions (20 trials in each direction). The operating pressure is $P_0 = 50$ kPa).
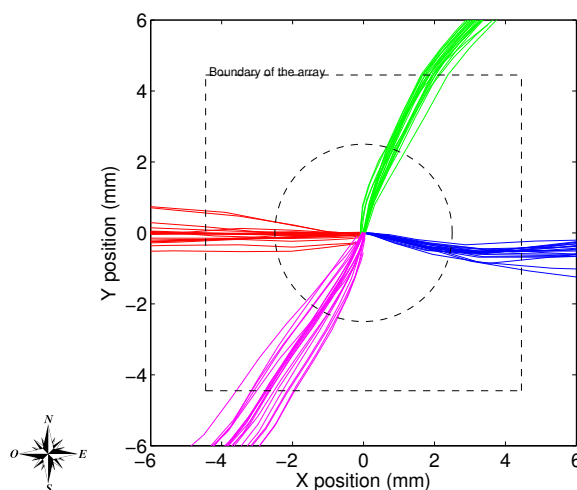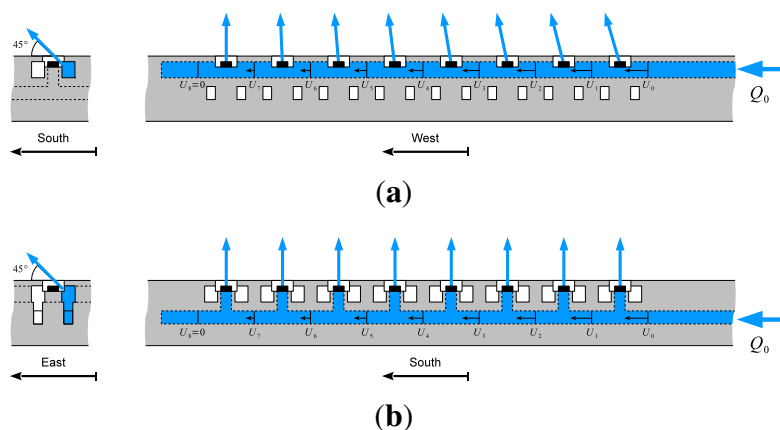

Figure 7. Illustration of the influence of the momentum given to geometry of nozzles. (**a**) Generation of jets towards south; (**b**) Generation of jets towards east.

(**a**)

(**b**)

If the nozzles are far enough from the pipe, it is assumed that the emerging fluid has lost all its axial momentum. However, in the north and south directions, the nozzles are drilled inside the channel itself. Due to this geometry, the fluid retains some of its axial momentum and the jet emerges at an angle of less than 90° in the downstream direction as shown by Bailey [16]. In the east and west directions the nozzles are 420 μm far from the pipe. This distance seems sufficient to get well oriented jets. For this reason, the trajectories in the north and south are deviated toward the direction of the air in the channels. To get well oriented jets in the north and south directions the device must be redesigned to keep the channels away from the nozzles.

The second conclusion of experiments presented in Figure 6 is that the object does not follow exactly the same path for a given direction. This may be due to air turbulence around the object and to the initial position of the object. Thus in the remaining of the paper, we will investigate mainly the east direction and always repeat 20 times the same experiment to get reliable measurement values.

3.3. Dynamic Model

With regards to the Reynolds number (around 100), the dynamic model of the object can be described as a mass receiving the drag force of a fully enclosing air flow:

$$m\ddot{x} = \frac{1}{2}\rho C_d A (v_{air} - \dot{x})^2 \tag{12}$$

where m is the mass of the object, C_d is the drag coefficient, A the reference area and v_{air} is the horizontal average speed of the air flow.

We do not know precisely the velocity field of the air flow in front of the object, but it is reasonable to assume that the average speed of the air flow v_{air} is proportional to the volume flow going through the micro-conveyor, such that:

$$v_{air} = \frac{Q_0}{S_{eq}} \tag{13}$$

S_{eq} is an equivalent surface that will be experimentally estimated.

The flow is controlled by a solenoid valve. To model the response time of the valve, we used a first order linear system with the time constant 0.008 (datasheet value) and unit gain. After the opening of the valve, the exiting air takes some time to reach its maximal speed. To take into account the time necessary to the establishment of the flow in the channels, we used another first order linear system with the time constant τ and unit gain.

3.4. Maximal Speed Evaluation

In order to identify the unknown parameters C_d, S_{eq} and τ of the dynamic model, we measured the position of the object along the east direction according to time for different supply pressures. Figure 8 shows a comparison between the modeled and the measured positions for two different pressures.

Figure 8. Comparison between dynamic model and experimental trajectories ($S_{eq} = 6.7096 \times 10^{-5}$ m^2, $\tau = 7$ ms). (**a**) $P_0 = 10$ kPa, $C_d = 1.2674$; (**b**) $P_0 = 40$ kPa, $C_d = 0.8763$.

(**a**)   (**b**)
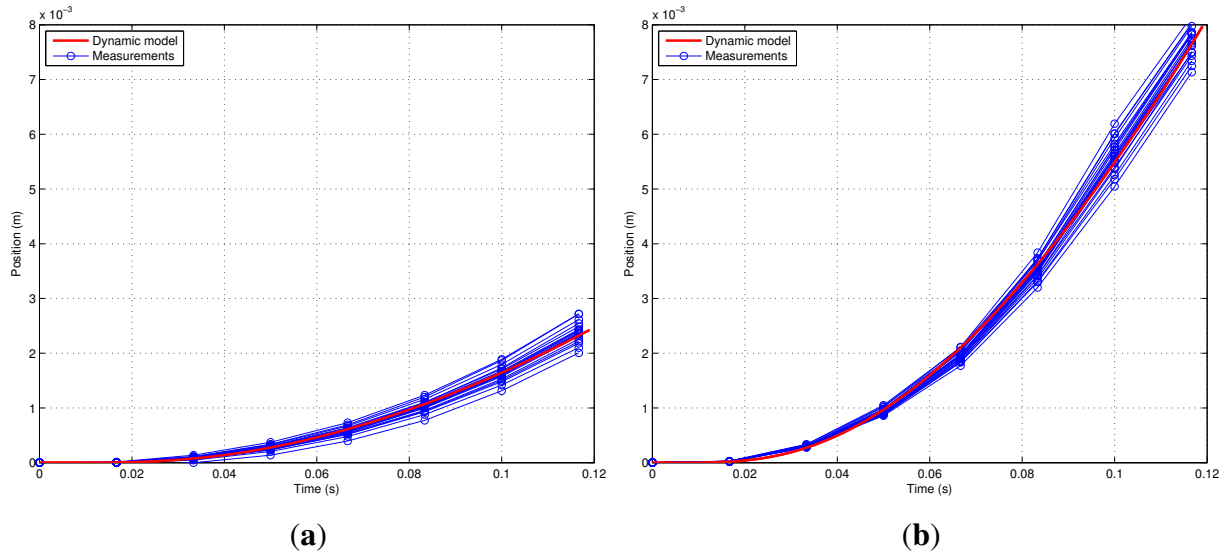
It is noteworthy that the obtained values of S_{eq} and τ can remain constant without loosing precision when the pressure changes as shown in Table 1. The time constant τ of the establishment of the flow is 7 ms. S_{eq} is equal to 6.71×10^{-5} m^2. The drag coefficient C_d decreases with the increase of the supply pressure. In general, C_d is not an absolute constant for a given body shape. It varies with Reynolds number R_e. For example, a smooth sphere has a C_d that varies from 1.5 for R_e around 50 to 1 for R_e around 150 [17]. The identified values of C_d are consistent with the usual values of C_d.

Table 1. Parameters of the dynamic model (least squares minimization) and object speeds.

P_0 (kPa)	10	20	30	40	50
LSE	1.48×10^{-6}	2.00×10^{-6}	11.58×10^{-6}	4.90×10^{-6}	10.14×10^{-6}
τ (ms)	7	7	7	7	7
S_{eq} (m^2)	6.71×10^{-5}	6.71×10^{-5}	6.71×10^{-5}	6.71×10^{-5}	6.71×10^{-5}
C_d	1.27	1.27	1.05	0.88	0.62
R_e	57	88	112	132	149
Measured output speed (mm·s^{-1})	44	92	120	140	137
Estimated maximal speed (mm·s^{-1})	175	268	341	402	456

These results validate the assumptions we made to establish the dynamic model. Thus, we can use the model to predict the maximal value of the object speed for a larger micro-conveyor as shown in Table 1. With the considered object, the operating pressure P_0 can not be set over 50 kPa. If the pressure is over 50 kPa, the object is ejected and does not move along the active direction. For this reason, we estimate that the object could reach a maximal speed of 456 mm·s^{-1} if several micro-conveyors were placed adjacent to each other.

4. Positioning Task

In this section, we focus on a positioning task. The aim is to evaluate the device in terms of resolution and repeatability.

4.1. Open-Loop Positioning

First, we tested the response to air pulses. An air pulse is defined by the operating pressure P_0, the duration T_p of the opening of the valves and the chosen direction (east, west, north, south). Figure 9 shows the position of the object in the X direction according to time for a single air pulse toward the east.

Figure 9. Position of the object according to time for a single air pulse toward the east (mean values on 20 tests). The solenoid valve is supplied when the bold line is equal to one. The pulse width is $T_p = 90$ ms. The operating pressure is $P_0 = 10$ kPa.
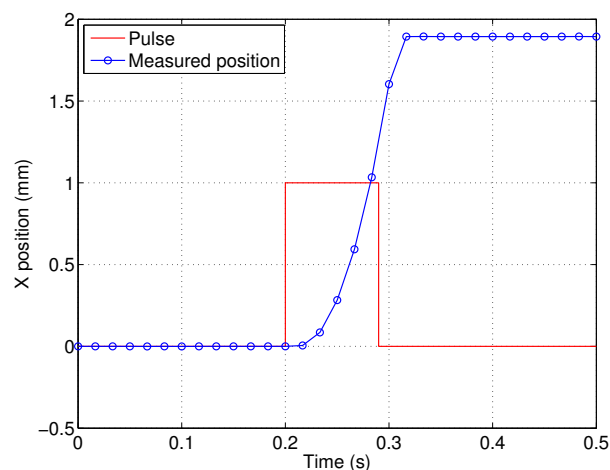

The response can be described by two different phases: the acceleration and the deceleration. The acceleration phase is identical to the response to a step. The deceleration phase is shorter than the acceleration's one. This is due to the friction that occurs between the object and the surface when the flow vanishes.

We observed the motion of the object for different pulse durations. The pressure and the initial object position were set to the same values (respectively 10 kPa and the center of the surface).

To evaluate precisely the range of reachable step size, we carried out many experiments with a large range of pulse durations (from 5 ms to 90 ms). Figure 10 shows the step size according to the duration.

The first thing to note is that the smallest step in the east direction is 0.3 µm. It is surprisingly small for a pneumatic manipulator. In the other directions, the smallest steps are in the same order of magnitude. Actually, as the object is lifted and pushed at the same time, the air cushion removes all dry frictions. Without frictions, there is no stick-slip effect that enables to reach this high resolution.

Figure 10. Step size toward the east according to the pulse duration (mean values and standard deviations on 20 tests). The operating pressure is $P_0 = 10$ kPa. (**a**) Linear scale; (**b**) Semi-logarithm scale.

(**a**)   (**b**)
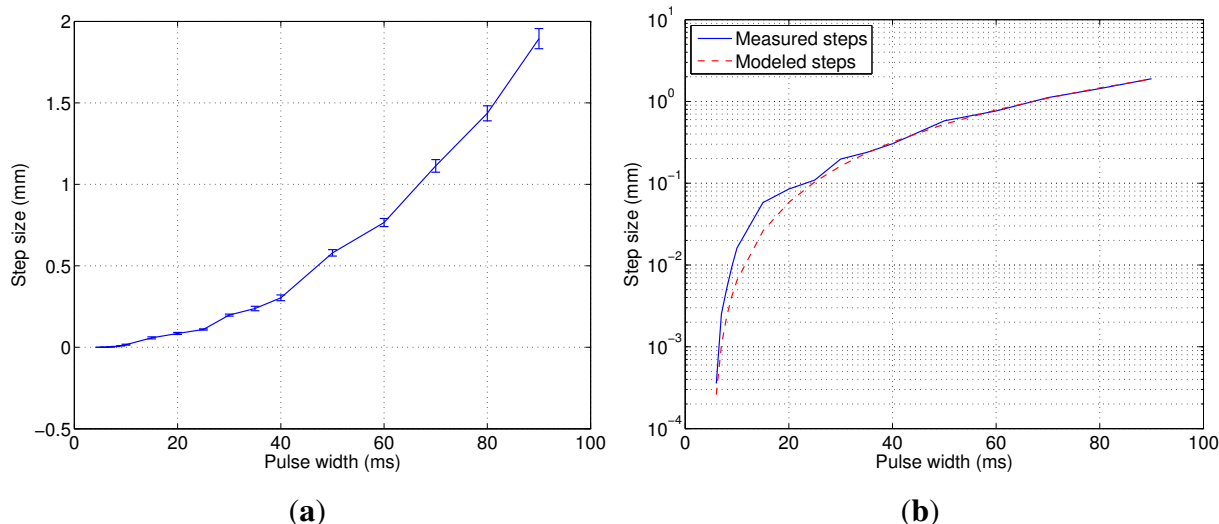
The second observation is that the step size increases with the square of the pulse duration. The fitted law is given by:

$$\Delta_{east}(T_p) = 0.00026(T_p - 5)^2 \tag{14}$$

with $\Delta_{east}(T_p)$ in millimeters and T_p in milliseconds.

This model is represented by the dashed line in Figure 10b. Below 5 ms the object does not move at all because the valve does not have enough time to open.

We carried out the same experiments in the three other directions and we obtained similar behaviors:

$$\Delta_{west}(T_p) = 0.00024(T_p - 5)^2 \tag{15}$$
$$\Delta_{north}(T_p) = 0.00010(T_p - 5)^2 \tag{16}$$
$$\Delta_{south}(T_p) = 0.00010(T_p - 5)^2 \tag{17}$$

The last conclusion is that the repeatability of the steps is not so good. We represented the standard deviation on the curve by vertical bars around the points (cf. Figure 10a). The average relative deviation is around 15% of the length of the step. This poor precision can be explained by the perturbations of the ambient air, by an heterogeneous distribution of the flow and by the motion of the object itself. For example, the pan and tilt angles of the object during the motion are not known. As the number of covered nozzles is not so high, the object may probably tilt during the motion and does not move flat. Different orientations can lead to different forces and then to different step sizes. For these reasons, it is not possible to position precisely the object using only open-loop control. To move the object exactly where we want, we need to measure the current position of the object and to apply a feedback control in order to reduce the position error.

4.2. Closed-Loop Position Control

The aim is to move the object at the center of the surface from arbitrary positions. The desired position (center) is noted (x_{ref}, y_{ref}). Thanks to the camera, the current position of the object is measured; it is noted (x, y). The position error is given by:

$$\begin{cases} e_x & = x_{ref} - x \\ e_y & = y_{ref} - y \end{cases} \tag{18}$$

According to the error between the measured position and the desired one, the valve is opened in order to carry the object to the desired position. For instance, if the object is localized at the north of the reference position, a south pulse is generated; if the object is localized at the east, a west pulse is generated; *etc*.

As the aim is to get the highest accuracy, we chose to modulate the width of the pulses as a function of the distance of the object to the target. Thanks to the previous measures, we can deduce the step size from the duration (direct model). So we can calculate the duration in order to get a step size corresponding to the position error (inverse model). Figure 11 details the feedback loop.

Figure 11. Feedback loop to control the abscissa of the object.
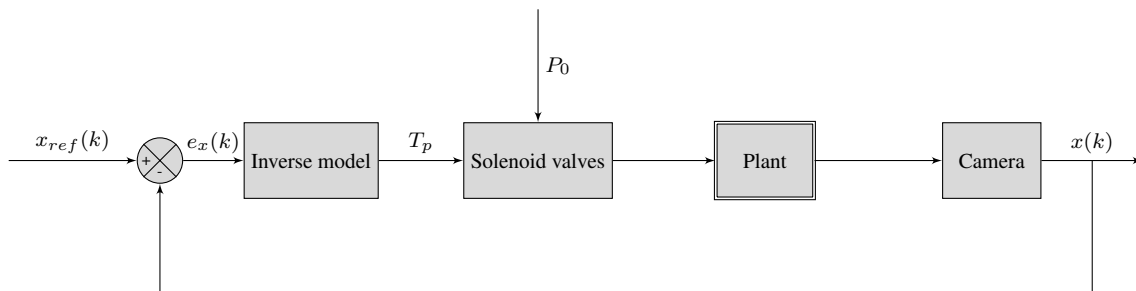
The inversion of Equations (14) and (15) gives for the X direction:

$$\begin{cases} T_{p,east} = 62\sqrt{e_x} + 5 & \text{if} \quad e_x > 0 \\ T_{p,west} = 64.5\sqrt{-e_x} + 5 & \text{else} \end{cases} \tag{19}$$

where $T_{p,east}$, $T_{p,west}$ are the durations of the pulse corresponding to the east and west directions.

Similar laws can be written for the Y direction:

$$\begin{cases} T_{p,north} = 100\sqrt{e_y} + 5 & \text{if} \quad e_y > 0 \\ T_{p,south} = 100\sqrt{-e_y} + 5 & \text{else} \end{cases} \tag{20}$$

We performed 20 trials from random positions to evaluate the positioning repeatability following ISO standard 9283 [18]. The positioning repeatability is defined by,

$$RP = \bar{l} + 3\sqrt{\frac{1}{n-1}\sum_{j=1}^{n}(l_j - \bar{l})^2} \tag{21}$$

l_j is the distance of the jth measure to the barycentre,

$$l_j = \sqrt{(x_j - \bar{x})^2 + (y_j - \bar{y})^2} \tag{22}$$

where $\bar{x}$ and $\bar{y}$ are the coordinates of the barycentre defined by $\bar{x} = \frac{1}{n}\sum_{j=1}^{n} x_j$ and $\bar{y} = \frac{1}{n}\sum_{j=1}^{n} y_j$. $\bar{l}$ is the mean distance to the barycentre defined by $\bar{l} = \frac{1}{n}\sum_{j=1}^{n} l_j$.

Figure 12 shows the trajectory of the object for each test. These experiments can be further appreciated in the video clip accompanying this paper. The positioning repeatability is 17.7 μm. This value is a lower bound of the accuracy we could obtain with the proposed feedback control.

Figure 12. Path of object from 20 arbitrary positions to the center of the surface with the feedback controller. (**a**) Large view; (**b**) close view.

(**a**)　　　　　　　　　　　　　　(**b**)
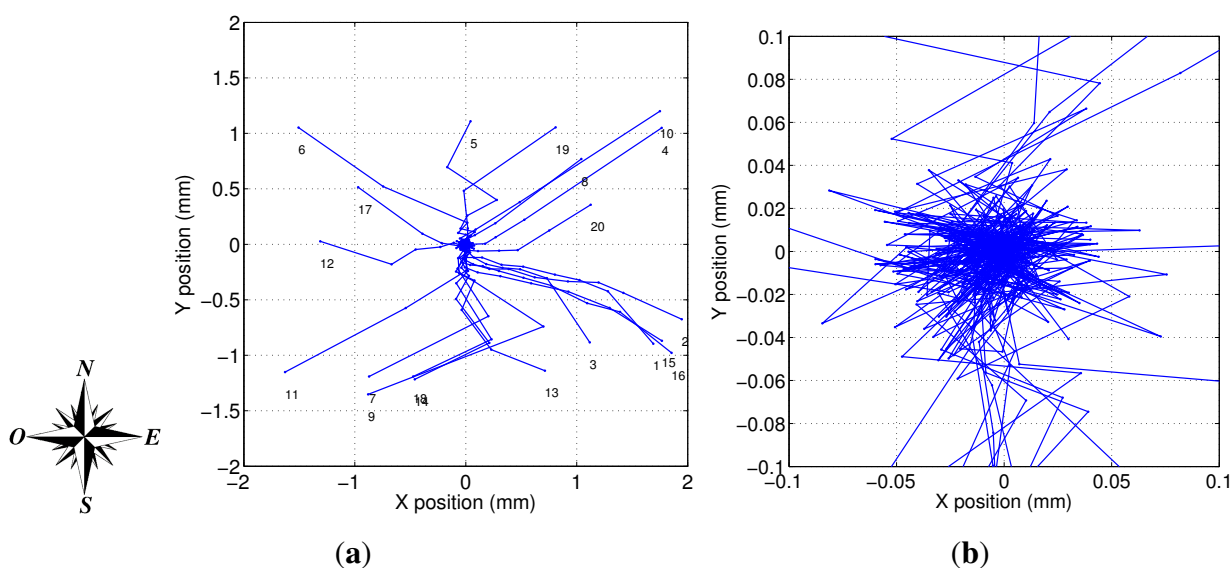
The object needs five steps on average to reach the final position. We could think that only one step is necessary since we used the inverse model to calculate the pulse width. The first explanation is the poor repeatability of the size of the step for a given pulse duration. The second one is that the model has been established in the center of the surface and performances are lower near the edges of the surface. So the first step is often shorter than expected as we can see in Figure 12. The last reason is that we did not take care of coupling. So when the object is near the center and for example both west and south directions are activated the amount of air is too high and the object overshoots the mark. Future works on the control could reduce the number of steps and maybe improve the positioning repeatability.

5. Conclusions

In this paper, we tested a micro-conveyor able to produce an array of tilted air jets. The performances are summed up in Table 2. It is noteworthy that this device is able to move the object with high speed relatively to its size and also to position it with a good precision. For instance, the object can reach a speed of up to 137 mm·s^{-1} in open loop whereas the positioning repeatability is around 5 μm with closed loop control. The smallest step the object can do is 0.3 μm (resolution). Moreover, we estimate that the speed could reach 456 mm·s^{-1} if several micro-conveyors were used to form a conveying line.

Table 2. Performances of the micro-conveyor.

Size of manipulated objects	1 mm to 10 mm
Maximal speed on one micro-conveyor	137 mm·s^{-1}
Estimated maximal speed on a line of micro-conveyors	456 mm·s^{-1}
Resolution (smallest step)	0.3 μm
Positioning repeatability (ISO 9283)	17.7 μm
Maximal air consumption	1.83 ls/min

Compared to existing devices, the micro-conveyor outperforms them in terms of speed and precision. Concerning the bandwidth, the device is in the middle range. During the experiments, we saw that the object reaches its maximal speed in about 100 ms before leaving the array. This settling time included the opening of the valve, the establishment of the flow and the behavior of the object in the flow. It could be improved in the future by using faster valves and shorter pipes.

Another advantage of the device is its sturdiness since a movable part does not exist inside the wafers. The valves require only conventional technologies that are cheap and robust.

Considering industrial applications, the upper space is free and enables the access for a robot to pick or place objects on the surface. We carried out some experiments with different kinds of objects which can be seen in the video clip accompanying this paper. The micro-conveyor can move cylindrical objects from 1 mm to 10 mm, but also various objects as electronic parts if the backside of the object is flat. In the future, we can imagine building large conveyor systems able to carry small parts at high speeds and to position them with a good accuracy when required.

Acknowledgments

Conflicts of Interest

The authors declare no conflicts of interest.

References

1. Luntz, J.E.; Messner, W.; Choset, H. Distributed manipulation using discrete actuator arrays. *Int. J. Robot. Res.* **2001**, *20*, 553–583.
2. Berlin, A.; Biegelsen, D.; Cheung, P.; Fromherz, M.; Goldberg, D.; Jackson, W.; Preas, B.; Reich, J.; Swartz, L.E. Motion Control of Planar Objects Using Large-Area Arrays of MEMS-Like Distributed Manipulators. Available online: http://citeseerx.ist.psu.edu/viewdoc/summary?doi=10.1.1.118.688 (accessed on 8 February 2014).

3. Biegelsen, D.K.; Berlin, A.; Cheung, P.; Fromherz, M.P.; Goldberg, D.; Jackson, W.B.; Preas, B.; Reich, J.; Swartz, L.E. Air-Jet Paper Mover: An Example of Meso-Scale MEMS. In Proceedings of the SPIE International Symposium on Micromachining and Microfabrication, Santa Clara, CA, USA, 18–19 September 2000.

4. Kim, Y.J.; Shin, D.H. Wafer Position Sensing and Motion Control in the Clean Tube System. In Proceedings of the IEEE International Conference on Industrial Technology, Mumbai, India, 15–17 December 2006; pp. 1315–1319.

5. Konishi, S.; Fujita, H. A conveyance system using air flow based on the concept of distributed micro motion systems. *J. Microelectromech. Syst.* **1994**, *3*, 54–58.

6. Fukuta, Y.; Chapuis, Y.A.; Mita, Y.; Fujita, H. Design, fabrication and control of MEMS-based actuator arrays for air-flow distributed micromanipulation. *J. Microelectromech. Syst.* **2006**, *15*, 912–926.

7. Guenat, O.T., Hirata, T., Akashi, T., Gretillat, M.A., and de Rooij, N.F. A pneumatic air table realized by micro-EDM. *J. Microelectromech. Syst.* **1998**, 7, 380–386.

8. Luntz, J.; Moon, H. Distributed Manipulation with Passive Air Flow. In Proceedings of the IEEE/RSJ International Conference on Intelligent Robots and Systems, Maui, HI, USA, 29 October–3 November 2001; pp. 195–201.

9. Moon, H.; Luntz, J. Distributed manipulation of flat objects with two airflow sinks. *IEEE Trans. Robot.* **2006**, *22*, 1189–1201.

10. Laurent, G.J.; Delettre, A.; Fort-Piat, N.L. A new aerodynamic traction principle for handling products on an air cushion. *IEEE Trans. Robot.* **2011**, *27*, 379–384.

11. Delettre, A.; Laurent, G.J.; Haddab, Y.; Fort-Piat, N.L. Robust control of a planar manipulator for flexible and contactless handling. *Mechatronics* **2012**, *22*, 852–861.

12. Yahiaoui, R.; Zeggari, R.; Malapert, J.; Manceau, J.F. A MEMS-based pneumatic micro-conveyor for planar micromanipulation. *Mechatronics* **2011**, *22*, 515–521.

13. Malapert, J.; Yahiaoui, R.; Zeggari, R.; Manceau, J.F. Tilted Micro Air Jet for Flow Control. In Proceedings of the European COMSOL Conference, Milano, Italy, 14–16 October 2009.

14. Zeggari, R.; Yahiaoui, R.; Malapert, J.; Manceau, J.F. Design and fabrication of a new two-dimensional pneumatic micro-conveyor. *Sens. Actuators A. Phys.* **2010**, *164*, 125–130.

15. Bradski, G. The OpenCV Library. Available online: http://opencv.org (accessed on 11 January 2014).

16. Bailey, B.J. Fluid flow in perforated pipes. *J. Mech. Eng. Sci.* **1975**, *17*, 338–347.

17. White, F.M. *Fluid Mechanics*; McGraw-Hill Science/Engineering/Math: New York, NY, USA, 2002.

18. *Manipulating Industrial Robots—Performance Criteria and Related Test Methods*; International Standard ISO 9283, Geneva, Switzerland, 1998.